Int. J. Electrochem. Sci., 12 **(2017)** 9575 – 9587, doi: 10.20964/2017.10.22

International Journal of
ELECTROCHEMICAL
SCIENCE
www.electrochemsci.org

A Comparative Study on Zn and Zn-Y Coatings on 42CrMo Steel by Pack Cementation Process

Li Liu, Sirong Yu[*]

College of Mechanical and Electronic Engineering, China University of Petroleum (East China), Qingdao, 266580, P.R China
[*]E-mail: liuli1212006@outlook.com, liuli1212006@126.com

Received: 20 May 2017 / *Accepted:* 28 July 2017 / *Published:* 12 September 2017

Zn and Zn-Y coatings on 42CrMo steel were prepared by pack cementation process at 360°C, 370°C, 380°C, 390°C and 400°C for 4 h, respectively. The purpose of this work was to comparatively study the differences on the microstructure and corrosion behavior between the two coatings. The relationship between the coating thickness and the temperature followed the linear rule. The Zn coating was continuous and had a single-layer structure. The Zn-Y coating exhibited a similar structure to the Zn-Fe coating. The Zn-Fe coating was a layer of Fe-Zn intermetallic compounds with increasing Fe_3Zn_{10} concentration. YZn_5 was formed with the addition of Y. The effect of Y addition on the microstructure and corrosion behavior of the Zn coating was discussed. The thickness of the Zn-Y coating was thicker than that of the Zn coating. The activation energy for the formation of the coating decreased with the addition of Y. The concentration of Fe_3Zn_{10} phase in the Zn-Y coating was slightly higher than that in the Zn coating, which suggested that the addition of Y promoted the formation of the Fe_3Zn_{10} phase. The immersion test showed that the addition of Y could improve the ability of the coating to resist the penetration of Cl^- and O_2.

Keywords: Zn; Pack cementation; Y; Microstructure; Corrosion

1. INTRODUCTION

Surface coating technologies are an effective means to improve the corrosion resistance of steel. Pack cementation process is one of the important surface coating technologies, which is an in situ chemical vapor deposition process used to prepare coating on substrate [1-3]. The process is economic, easy to operate, and suitable to be applied on substrates with complex shapes [4, 5].

Pack cementation Zn coating acting as sacrificial anode material has been developed to improve the corrosion resistance of steel [6]. However, the single Zn coating can not satisfy the need

of serious corrosion environment. The codeposition of two elements by pack cementation process has been put forward in recent years. The codeposition process not only can take full advantages of each element, and can also let the substrate surface acquire better performance. The codeposition of two elements is the most popular technology [7, 8]. The codeposition of Zn and Al has been applied in improving the properties of single Zn coating. The microstructure evolution and corrosion resistance of the pack cementation Zn and Zn-Al coatings on AISI 1020 steel were reported by Qi et al [9]. They found that the Zn-Al coating exhibited better corrosion resistance. The corrosion behaviors of Zn-Al coating and Zn coating on a commercial carbon steel in aqueous solutions and high-temperature environment have been studied by He et al [10]. They found that compared with the Zn coating, the Zn-Al coating had better corrosion resistance in both two environments. It is obvious that the codeposition of Zn and other element has a great potential for improving microstucture and performance of Zn coating. Many researches have reported that the codeposition of Al and a small amount of rare earth element Y or its oxide Y_2O_3 was an effective means to improve the oxidation resistance of the pack cementation coating at high temperature [11-14]. However, there is relatively little research on the codeposition of Zn and Y. In this work, Zn coatings and Zn-Y codeposition coatings on 42CrMo steel were prepared by the pack cementation at different temperatures (from 360°C to 400°C). The goal of this work is to comparatively study the differences on the microstructure and corrosion behavior between the two coatings.

2. EXPERIMENTAL

42CrMo steel used as substrate was cut into specimens with a dimension of 3mm × 10mm × 10mm. The specimens were ground with 2000 grid SiC paper, washed with alcohol, and dried with warm flowing air. The chemical compositions of the 42CrMo steel are shown in Table 1.

Table 1. Compositions of 42CrMo steel (wt.%)

C	Si	Mn	Mo	Cr	Cu	Ni	S	P	Fe
0.45	0.35	0.80	0.24	1.10	0.02	0.02	0.03	0.03	96.96

The conventional pack cementation process was used in this work. The pack mixture for the preparation of Zn coating was composed of Zn powder as source element and NH_4Cl powder as activator. Zn-Y coating was obtained by the addition of Y_2O_3 to the pack mixture. The specimen was embedded in the pack mixture in an Al_2O_3 crucible. The filled crucible was sealed with high temperature resistant sand and then placed into a furnace with a heating rate of $15°C \cdot min^{-1}$. The crucible was heated to the desired temperature and held at this temperature for 4 h. Then the crucible was cooled in the furnace to room temperature. The furnace was filled with inert gas during the heating process. The temperature and composition of the pack mixture are shown in Table 2.

Table 2. Temperature and composition of pack mixture

Coating	Temperature (°C)	Composition (wt.%)		
		Zn	Y_2O_3	NH_4Cl
Zn	360	98	0	2
	370	98	0	2
	380	98	0	2
	390	98	0	2
	400	98	0	2
Zn-Y	360	96	2	2
	370	96	2	2
	380	96	2	2
	390	96	2	2
	400	96	2	2

The cross-sectional microstructure of coated specimens was observed using optical microscopy (OM) and scanning electron microscopy (SEM) equipped with energy dispersive spectroscopy (EDS). The phases of the coating's surface were analyzed using X-ray diffraction (XRD) technique. The coating thickness was derived from the OM graphs.

The corrosion resistance of the substrate and coated specimens was evaluated by immersion test. The specimens were scratched by a knife in x-shape, and then immersed in 3.5 wt.% NaCl solution for a specified period of time (30 days). The corrosion morphology was observed using a digital camera. The phases of the corrosion products were analyzed using XRD. The cross-sectional corrosion morphology was observed using SEM. The polarization behavior of the uncoated and coated specimens in NaCl solution were evaluated using the CS350 electrochemical workstation. The specimen and the Pt mesh were used as the working electrode and the counter electrode, respectively. The working area of the specimen was 5 mm^2. The saturated calomel electrode was used as the reference electrode. The scan rate was 1 mV/s. In order to stabilize potential, the opening circuit potential was measured for 20 minutes. Then the polarization test began.

3. RESULTS AND DISCUSSION

3.1 Microstructure

The cross-sectional microstructures of Zn coatings are shown in Figure 1. There is a clear interface between the coating and the substrate, which implies that the formation of the coating is due to diffusion [12]. There are no visible pores or cracks at the interface, which illustrates that the coating has a good adhesion to the substrate. The Zn coatings are continuous and have a single-layer structure. No penetrating crack is found in the coatings. But some microcracks are found in the outer part of the coating. The coating thickness gradually increases with the increase of temperature. The coating prepared at high temperature is more uniform than that prepared at low temperature. The edge of the coating is jagged, which shows that the coating surface is rough and uneven. The irregularity decreases with the increase of temperature, which shows that the coating surface is improved with the increase of

temperature.

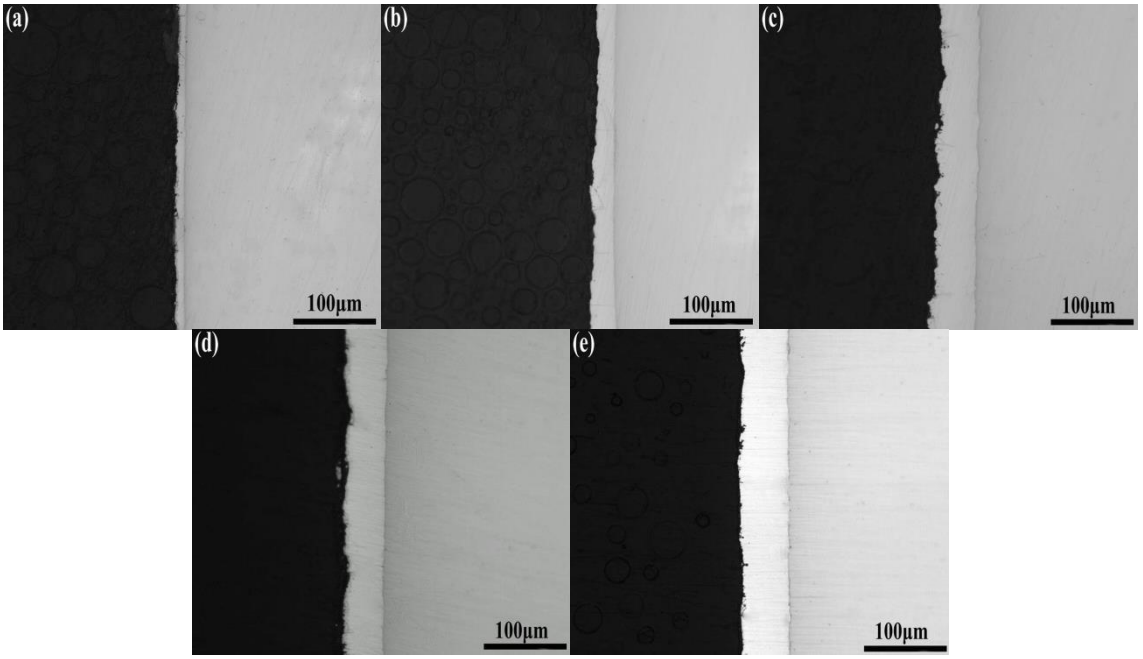

Figure 1. Cross-sectional microstructures of Zn coatings prepared at different temperatures,(a) 360°C, (b) 370°C, (c) 380°C, (d) 390°C, (e) 400°C

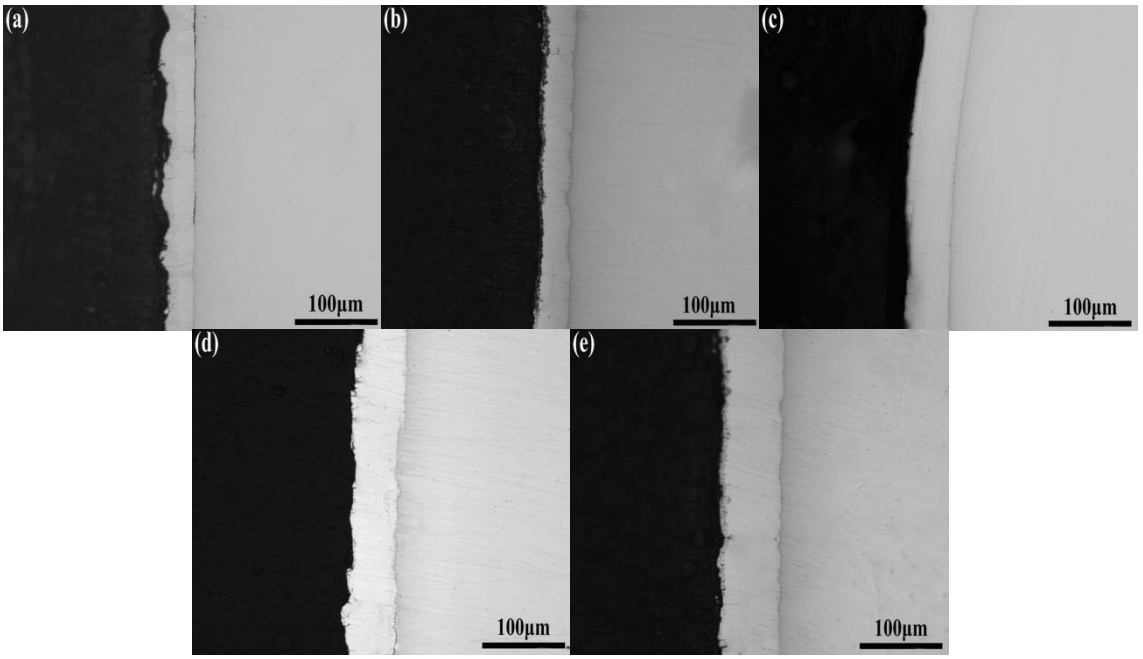

Figure 2. Cross-sectional microstructures of Zn-Y coatings prepared at different temperatures,(a) 360°C, (b) 370°C, (c) 380°C, (d) 390°C, (e) 400°C

The cross-sectional microstructures of Zn-Y coatings are shown in Figure 2. The microstructure of the Zn-Y coating is similar to that of the Zn coating. No defects are found in the

interface. The microcracks in the outer part of the Zn-Y coating are less than those in the outer part of the Zn coating. The thickness of the Zn-Y coating clearly increases with the increase of temperature. At a same temperature, the Zn-Y coating is thicker and more uniform than the Zn coating, which implies that the addition of Y can improve the quality of the Zn coating. The thickness uniformity of the Zn-Y coating increases with the increase of temperature, which shows that the increase of temperature also can improve the quality of the Zn-Y coating.

The thicknesses of the Zn and Zn-Y coatings are shown in Figure 3. The thicknesses of the Zn coatings prepared at 360°C, 370°C, 380°C, 390°C and 400°C are 8.7 μm, 18.8 μm, 25.1 μm, 35.7 μm and 54.7 μm, respectively. The thicknesses of the Zn-Y coatings prepared at 360°C, 370°C, 380°C, 390°C and 400°C are 26.2 μm, 34.4 μm, 44.7 μm, 50.2 μm and 61.2 μm, respectively. It is concluded that the coating thickness can be increased by increasing temperature and adding Y. As shown in Figure 3, the relationship between the thickness and the temperature follows the linear rule. According to the fitting result, the growth kinetic of the Zn coating can be expressed by the following equation:

$$x = 1.09T - 385.22 \quad (1)$$

where x is the coating thickness and T is the temperature. The growth kinetic of the Zn-Y coating can be described by the following equation:

$$x = 0.87T - 287.04 \quad (2)$$

When x=0, the temperatures for the formation of Zn coating and Zn-Y coating are 353.41°C and 329.93°C, respectively. It can be concluded the addition of Y reduces the temperature needed for the formation of the coating. After calculation, the thickness of Zn coating equals the thickness of Zn-Y coating when the temperature is 446.27°C. This temperature is higher than the melting point of Zn (419.53°C). Therefore, it can be concluded that the addition of Y plays a thickening effect in the pack Zn-Fe coating formation temperature range. The thickness difference between the Zn-Y coating and the Zn coating decreases with the increase of temperature, which shows that the thickening effect of Y is better at low temperature.

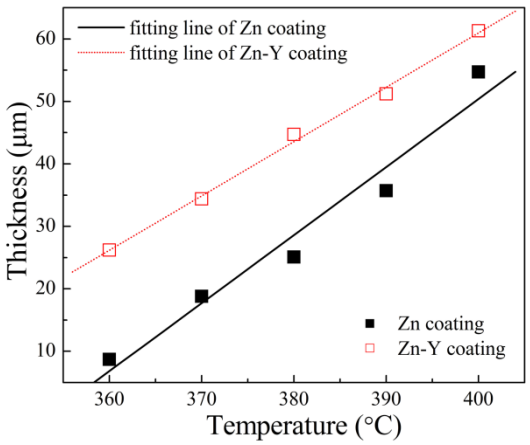

Figure 3. Thickness of Zn and Zn-Y coatings prepared at different temperatures

The relationship between the natural logarithm (ln) of thickness (x) and $T_a^{-1} \times 1000$ is shown in

Figure 4. According to the fitting results, the formation of the Zn and Zn-Y coatings is well consonant with the Arrhenius relationship, which confirmed that the formation of Zn and Zn-Y coatings is due to diffusion. The relationship between the temperature and the coating thickness can be described by the equation below [15, 16]:

$$\ln x = -E/(RT) + \ln A \qquad (3)$$

where E is the activation energy, R is the gas constant (8.314 $J \cdot mol^{-1} \cdot K^{-1}$), T_a is the absolute temperature, and A is a constant. The fitting lines of Zn coating and Zn-Y coating give slopes of -18.44 and -8.96, respectively. The activation energies can be computed by substituting the slopes into Eq. (3). The activation energies are 153.31 $kJ \cdot mol^{-1}$ and 74.49 $kJ \cdot mol^{-1}$ for the formation of the Zn coating and the Zn-Y coating, respectively. It is obvious that the activation energy for the formation of Zn coating is much larger than that for the formation of Zn-Y coating, so it is concluded that the addition of Y can greatly reduce the activation energy.

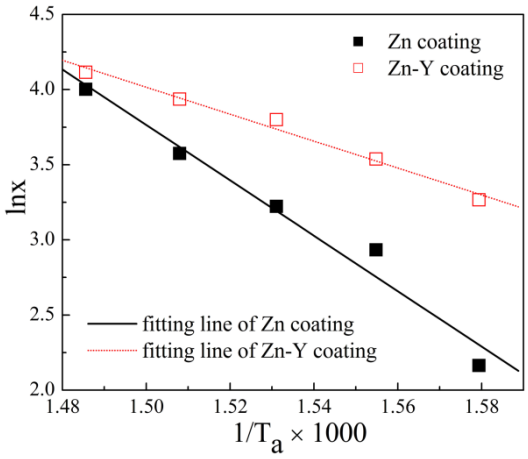

Figure 4. Relationship between lnx and $T_a^{-1} \times 1000$

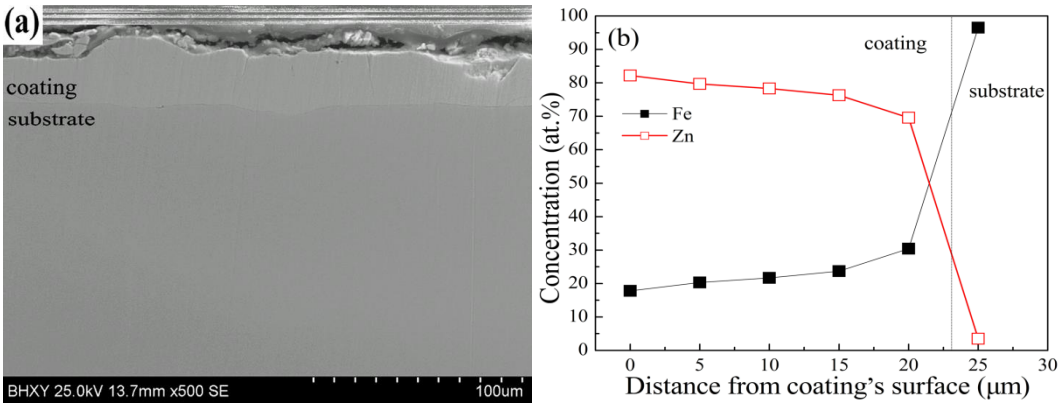

Figure 5. Cross-sectional SEM image (a) and element concentration profile (b) of Zn coating prepared at 370°C

The cross-sectional SEM image and element concentration profile of the Zn coating prepared at

370°C are shown in Figure 5. As shown in Figure 5a, the edge of the coating is jagged and crumbling, which is similar to the result depicted in Figure 1. The crumblings are in the form of sheets and bulk. According to Figure 5b, starting from surface, the Zn coating is a Zn-Fe alloy with increasing Fe concentration. The concentration of Fe in the coating ranges from 17.81 at.% to 23.74 at.%. The formation of the Zn coating is due to the inward diffusion of Zn atoms and the outward diffusion of Fe atoms. A small amount of Zn atoms have diffused into the substrate, which indicates that the outward diffusion of Fe was accompanied by the inward diffusion of Zn. At the interface between the coating and the substrate, the concentration of Fe changes a lot.

The cross-sectional SEM image and element concentration profile of the Zn-Y coating prepared at 370°C are shown in Figure 6. According to the SEM images, the edge of the Zn-Y coating is obviously flatter than the Zn coating No big crumblings are found in the edge of the Zn-Y coating, which shows that the coating surface is improved with the addition of Y. The result is consistent with that depicted in Figure 2. The Zn-Y coating is composed of large amounts of Zn atoms, small amounts of Fe atoms and trace amounts of Y atoms. From surface to interior, the concentration of Fe in the coating ranges from 18.27 at.% to 34.57 at.%. Compared with Figure 5b, the concentration of Fe in the coating and the concentration of Zn in the substrate increase with the addition of Y. It is concluded that the addition of Y promotes the inward diffusion of Zn atoms and the outward diffusion of Fe atoms. The concentration of Y in the Zn-Y coating surface is about 0.15 at.%, which changes to 0.22 at.% in the interface. A trace amount of Y atoms have diffused into the substrate to a depth of several microns.

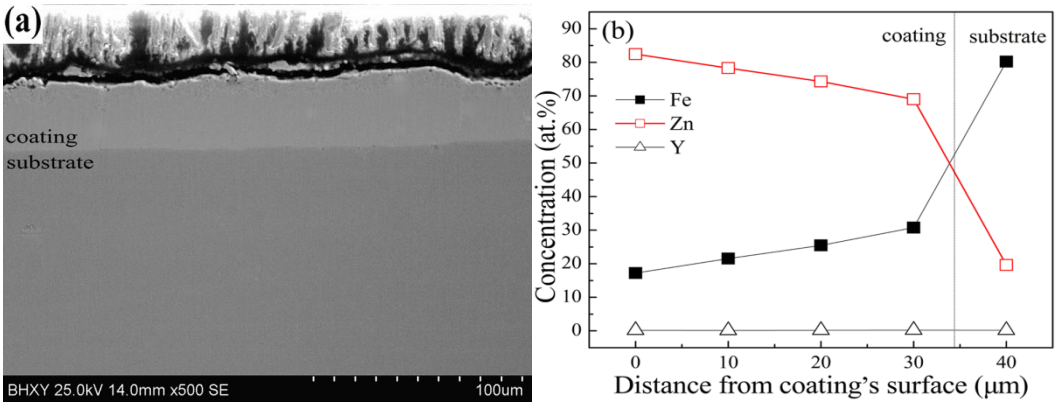

Figure 6. Cross-sectional SEM image (a) and element concentration profile (b) of Zn-Y coating prepared at 370°C

The XRD patterns of the coatings' surface are shown in Figure 7. The phases of the Zn coating are mainly δ-$FeZn_{10}$ and Γ-Fe_3Zn_{10}. The XRD result is fit to the Fe-Zn binary phase diagram [6, 17]. YZn_5 phase is formed with the addition of Y, which implies that Y took part in the formation of the Zn-Y coating. It can be concluded that the codeposition of Zn and Y was achieved. As shown in Figure 5b, the surface of the Zn coating is composed of 82.19Zn-17.81Fe (at.%). According to Figure 6b, the surface of the Zn-Y coating is composed of 81.58Zn-18.27Fe-0.15Y (at.%). By calculation, the

concentration of Fe_3Zn_{10} phase in the coating's surface is much higher than the $FeZn_{10}$ phase. The concentration of Fe_3Zn_{10} phase in the Zn-Y coating is slightly higher than that in the Zn coating, which suggests that the addition of Y promoted the formation of the Fe_3Zn_{10} phase. From surface to interior, the concentration of Fe increases gradually, which implies that the amount of Fe_3Zn_{10} in the coating's interior is higher than that in the coating's surface. That is, the Zn coating is a layer of Fe-Zn intermetallic compounds with increasing Fe_3Zn_{10} concentration. According to previous studies [18, 19], the brittle $FeZn_{10}$ phase facilitates the propagation of the microcrack but the ductile Fe_3Zn_{10} phase prevents the microcrack from propagating. That is, with the increase of the concentration of Fe_3Zn_{10} phase in the coating, the amounts of the microcracks in the coating decreases. In other words, the quality of the coating is improved with the addition of Y. The result is consistent with that from the SEM images.

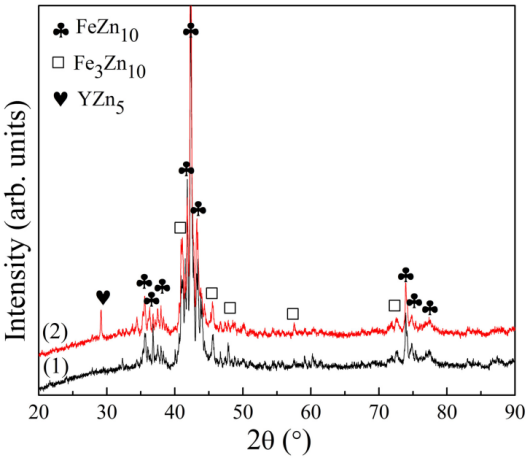

Figure 7. XRD patterns of surface of different coatings prepared at 370°C (1) Zn coating, (2) Zn-Y coating

3.2 Corrosion resistance

The corrosion morphologies of the substrate and the coatings prepared at 370°C are shown in Figure 8. The surface of the substrate is covered with a layer of red rusts. The rusts are loose and easy to fall off, which can not reduce the corrosion of the substrate. No red rust is found in the coatings' surface. The whole surface of the Zn coating is covered by a layer of white powders. The dotted distribution of the corrosion products is due to the selective dissolution of Zn [20]. The x-shape scratch can be faintly visible. The white powder layer is denser than the red rust layer and it has good adhesion with the coating, which implies that the corrosion products layer can retard the corrosion. For the Zn-Y coating, less white powders are found in the surface, and the x-shape scratch is clearly visible. The Zn-Y coating still exhibits its original grey color. It can be concluded that the corrosion resistance of Zn-Y is better than that of the Zn coating. That is, the addition of Y can enhance the corrosion resistance of Zn-Fe coating.

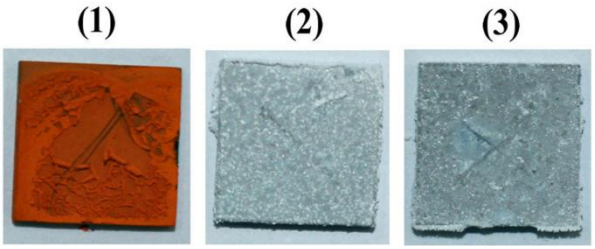

Figure 8. Corrosion morphologies of substrate and coatings prepared at 370°C (1) substrate, (2) Zn coating, (3) Zn-Y coating

The XRD patterns of corrosion products on the coatings' surface are shown in Figure 9. The corrosion products are composed of $Zn_5(OH)_8C1_2{\cdot}H_2O$, $Zn(OH)_2$ and ZnO. The similar corrosion products have been reported in other studies [20, 21]. The corrosion of Zn in the NaCl solution is controlled by oxygen absorption corrosion. $Zn(OH)_2$ was firstly formed through the oxygen absorption corrosion reaction. With the penetration of Cl^-, $Zn_5(OH)_8Cl_2{\cdot}H_2O$ was formed. No iron oxides are found in the corrosion products, which implies that the coating can effectively prevent the Fe from corrosion.

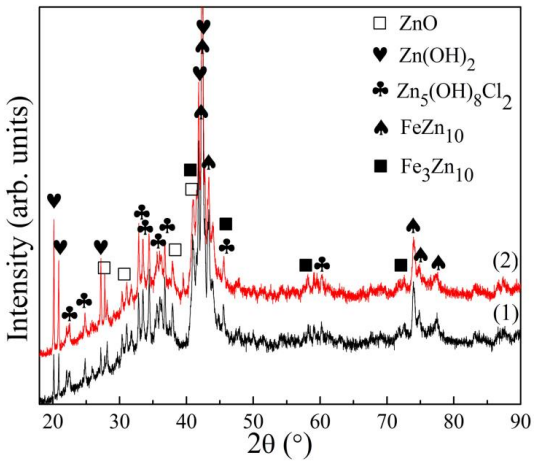

Figure 9. XRD patterns of corrosion products on coatings' surface (1) Zn coating, (2) Zn-Y coating

The cross-sectional corrosion morphologies of the Zn and Zn-Y coatings formed at 370°C are shown in Figure 10. The chemical compositions of the marked points revealed by EDS are listed in Table 3. The upper portion of the Zn coating is corroded seriously. Many long cracks are found in the coating, which are the channels of the penetration of Cl^- and O_2. Only some small corrosion holes are found in the Zn-Y coating. The cracks in the Zn-Y coating are significantly less than those in the Zn coating. It is obvious that the corrosion of Zn coating is more serious than that of the Zn-Y coating, which is consist with the result revealed by Figure 7. According to Table 3, the amounts of O and Cl in the corrosion region of the Zn-Fe coating are much larger than those in the Zn-Y coating, which implies that the resistance of the Zn-Y coating to the penetration of Cl^- and O_2 is better than that of the

Zn coating. The better ability of the Zn-Y coating to resist the penetration of Cl^- and O_2 can be explained as follows.

Firstly, according to the SEM images, the microstructure of the coating was improved with the addition of Y. The phase containing Y (YZn_5) mainly distributed in the interface and grain boundaries [22, 23], which can reduce the defects and increase the compactness of the coating. Thus the resistance of the Zn-Y coating to the penetration of Cl^- and O_2 increased. Secondly, the corrosion products film on the Zn-Y coating was more stable than that on the Zn coating. The YZn_5 formed in the boundaries could improve the adhesion between the coating and the corrosion product film. Thus the corrosion product film played as the barrier between the coating and the corrosion solution could effectively prevent the Zn-Y coating from corrosion. The similar behavior of rare earth element has been reported in other studies [24, 25]. Thirdly, the better resistance to the penetration of Cl^- and O_2 is due to the more Fe_3Zn_{10} phase in the Zn-Y coating. It has been mentioned that the Fe_3Zn_{10} phase could prevent the spread of cracks. As the cracks are the channels for the penetration of Cl^- and O_2, the Zn-Y coating containing more Fe_3Zn_{10} phase exhibited the better resistance to the penetration.

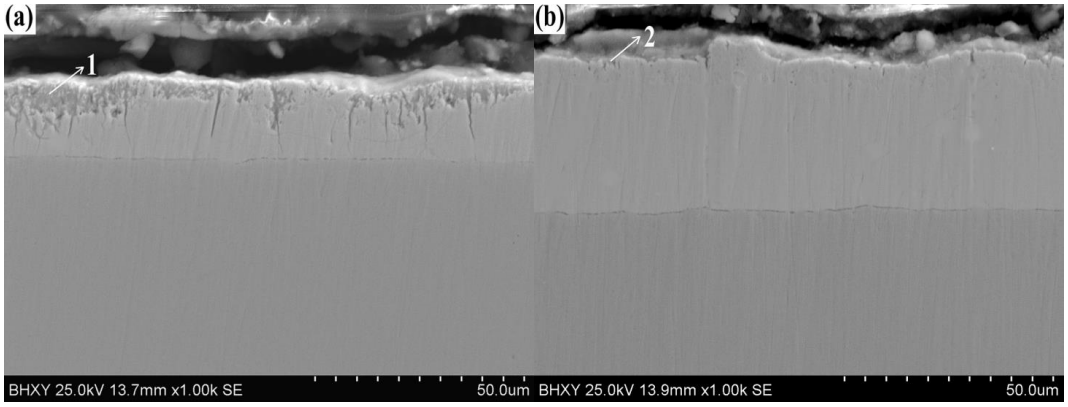

Figure 10. Cross-sectional corrosion morphologies of coatings prepared at 370°C (a) Zn coating, (b) Zn-Y coating

Table 3. EDS analysis results of the marked points in Figure 10

Point	Composition (at.%)				
	Fe	Zn	O	Cl	Y
1	17.63	42.70	30.57	9.09	0
2	18.18	55.08	21.56	5.18	0.14

The polarization curves of the substrate and the coatings prepared at 370°C are shown in Figure 11. The corrosion potential (E_{corr}), corrosion current density (i_{corr}), polarization resistance (R_p) and Tafel slope are shown in Table 4. The R_p was calculated by the following equation [26]:

$$R_p = \beta_a\beta_c/(2.303i_{corr}(\beta_a+\beta_c)) \quad (4)$$

where β_a is the anodic Tafel slope and β_c is the cathodic Tafel slope.

The i_{corr} value of the substrate is 1.57×10^{-2} mA/cm^2. The i_{corr} values of the Zn coating and the

Zn-Y coating are 1.43×10^{-3} mA/cm^2 and 1.84×10^{-4} mA/cm^2, respectively. Smaller corrosion current density value means better corrosion resistance [27]. It is obvious that the corrosion resistance of the coating is better than the substrate. The corrosion resistance of the Zn-Y coating is better than that of the Zn coating. The result is consist with that from the immersion test. The E_{corr} value of the substrate is -745.98 mV. The E_{corr} values of the Zn coating and the Zn-Y coating are -1123.72 mV and -1003.14 mV, respectively. It can be found that the coating plays a role in protecting cathode. The β_a values of the Zn coating and the Zn-Y coating are obviously smaller than that of the substrate, which shows that the corrosion products layers on the coatings could prevent the corrosion to some extent. The result agrees with that from the corrosion morphologies. The R_p values has a same trend as the β_a values.

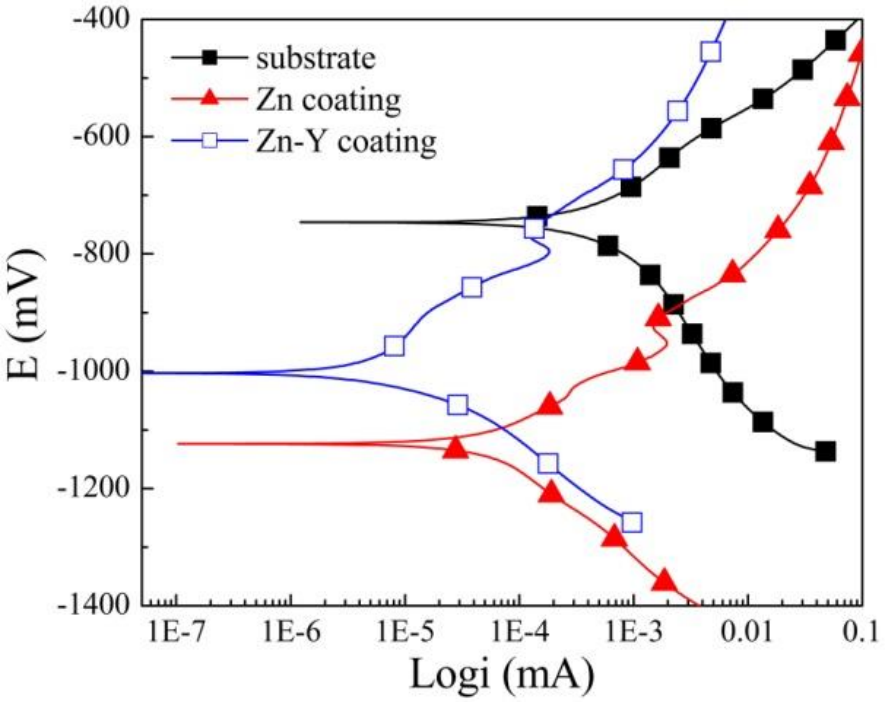

Figure 11. Polarization curves of substrate and coatings prepared at 370°C

Table 4. Corrosion potential, corrosion current density, polarization resistance and Tafel slopes

specimen	E_{corr} (mV)	i_{corr} (mA/cm^2)	β_a (mV/decade)	β_c (mV/decade)	R_p ($\Omega\cdot$cm^2)
substrate	-745.98	1.57×10^{-2}	224.63	275.41	3.42×10^{3}
Zn coating	-1123.72	1.43×10^{-3}	131.49	172.31	3.24×10^{4}
Zn-Y coating	-1003.14	1.84×10^{-4}	107.54	149.43	2.72×10^{5}

4. CONCLUSIONS

(1) Zn and Zn-Y coatings on 42CrMo steel were achieved by pack cementation at 360°C, 370°C, 380°C, 390°C and 400°C for 4 h, respectively. The coating exhibited a single-layer structure.

The coating thickness increased with the increase of temperature.

(2) The relationship between the thickness and the temperature followed the linear rule. The addition of Y could increase coating thickness. The thickening effect of Y was better at low temperature.

(3) The addition of Y could decrease the activation energy. The activation energies were 153.31 $kJ \cdot mol^{-1}$ and 74.49 $kJ \cdot mol^{-1}$ for the formation of the Zn coating and the Zn-Y coating, respectively.

(4) The Zn coating consisted of $FeZn_{10}$ and Fe_3Zn_{10} phases. The Zn coating was a layer of Fe-Zn intermetallic compounds with increasing Fe_3Zn_{10} concentration. YZn_5 was formed with the addition of Y. The addition of Y promoted the formation of Fe_3Zn_{10} phase, but retarded the formation of $FeZn_{10}$ phase.

(5) The Zn and Zn-Y coatings could prevent the substrate from corrosion. The resistance of the Zn-Y coating to the penetration of Cl^- and O_2 was better than that of the Zn coating.

ACKNOWLEDGEMENT
This work was supported by the Fundamental Research Funds for the Central Universities (16CX06020A).

References

1. S. A. Tsipas and E. Gordo, *Mater. Charact.*, 118 (2016) 494.
2. J. Kipkemoi and D. Tsipas, *J. Mater. Sci.*, 31(1996) 6247.
3. D. Zeng, S. Yang and Z. D. Xiang, *Appl. Surf. Sci.*, 258 (2012) 5175.
4. Z. L. Mao, X. J. Yang, S.L. Zhu, Z. D Cui and Y. Lu, *Surf. Coat. Technol.*, 254 (2014) 54.
5. D. Stathokostopoulos, D. Chaliampalias, E. C. Stefanai, G. Polymeris, K. Chrissafis, E. Hatzikraniotis, K. M. Paraskevopoulos and G. Vourlias, *Appl Surf Sci.*, 285 (2013) 417.
6. A. R. Marder, *Prog. Mater. Sci.*, 45 (2000) 191
7. Z. D. Xiang and P. K. Datta, *Mater. Sci. Eng. A.*, 363 (2003) 185.
8. X. Tian and X. Guo, *Surf. Coat. Technol.*, 203 (2009) 1161.
9. Q. Xue, Y.S. Cai, J. Y. Yu, L. Huang, J. Wei and J. Zhang, *J. Alloys. Compd.*, 699 (2017) 1012.
10. Y. He, D. Li, D. Wang, Z. Zhang, H. Qi and W. Gao, *Mater. Lett.*, 56 (2002) 554.
11. X. Zhao and C. Zhou, *Corros. Sci.*, 86 (2014) 223.
12. P. Zhang and X. Guo, *Sur. Coa. Technol.*, 206 (2011) 446.
13. J. Xu, A. Liu, Y. Wang and Y. Zhou, *Rare. Metal. Mat. Eng.*, 45 (2016) 1413.
14. A. L. Liu, J. H. Sui, Y. C. Lei, W. Cai, Z. Y. Gao and L. C. Zhao, *J. Mater. Sci.*, 42 (2007) 5791.
15. Q. Min and C. Zhou, *Surf. Coat. Technol.*, 206 (2012) 2899.
16. Z. D. Xiang and P. K. Datta, *Surf. Coat. Technol.*, 184 (2004) 108.
17. B. Peng, J. Wang, X. Su, Z. Li and F. Yin, *Surf. Coat. Technol.*, 202 (2008) 1785.
18. N. L. Okamoto, D. Kashioka, M. Inomoto, H. Inui, H. Takebayashi and S. Yamaguchi, *Scr. Mater.*, 69 (2013) 307.
19. G. Vourlias, N. Pistofidis, D. Chaliampalias, E. Pavlidou, P. Patsalas, G. Stergioudis, D. Tsipas and E. K. Polychroniadis, *Surf. Coat. Technol.*, 200 (2006) 6594.
20. H. Katayama and S. Kuroda, *Corros. Sci.*, 76 (2013) 35.
21. T. E. Graedel, *J. Electrochem. Soc.*, 136 (1989) 193.
22. W.Yu, J. Tian, W. Tian, J. Zhao, Y. Li and Y. Liu, *J. Rare. Earth.*, 33 (2015) 221.

23. L. J. Shang, *Rare. Metal.*, 19 (1995) 132.
24. T. J. Luo, Y. S. Yang, Y. J. Li and X. G. Dong, *Electrochim. Acta.*, 54 (2009) 6433.
25. X. Xing, H. Wang, P. Lu and Z. Han, *Surf, Coat, Technol.*, 291(2016) 151.
26. F. Wei, W. Zhang, T. Zhang and F. Wang, *Int. J. Electrochem. Sci.*, 12 (2017) 155.
27. D. Zhou, J. Wang, Y. Gao, and L. Zhang, *Int. J. Electrochem. Sci.*, 12 (2017) 192.